

Analytical catch-slip bond model for arbitrary forces and loading rates

J. T. Bullerjahn and K. Kroy*

Universität Leipzig, Institut für Theoretische Physik, Postfach 100 920, D-04009 Leipzig, Germany

(Received 23 October 2015; published 11 January 2016)

Some biological bonds exhibit a so-called catch regime, where the bond strengthens with increasing load. We build upon recent advances in slip-bond kinetics to develop an analytically tractable, microscopic catch-slip bond model. To facilitate the analysis of force-spectroscopy data, we calculate the bond's mean lifetime and the rupture-force distribution for static loading and linear force ramps. Our results are applicable for arbitrary forces and loading rates, covering the whole range of conditions found in experiments and all-atom simulations. A generalization to account for force transducers of finite stiffness is also provided.

DOI: [10.1103/PhysRevE.93.012404](https://doi.org/10.1103/PhysRevE.93.012404)**I. INTRODUCTION**

Noncovalent bonds play a crucial role in biomaterial stabilization, e.g., by preserving the tertiary structure of proteins [1] and guaranteeing the integrity of polymer networks [2]. They are also responsible for the formation of receptor-ligand complexes, such as in focal adhesions [3], that allow cells and bacteria to adhere to surfaces and extracellular scaffold structures. In recent years, the binding kinetics of these bonds has been studied on a single molecule level by repeatedly exposing the bond to external forces and thus inducing a series of unbinding events [4]. Experimentalists usually either probe the bond's lifetime under static loads [5,6] or measure the force at which the bond yields when the force is gradually ramped up [7,8]. However, due to various technical limitations, the forces and loading rates typically realized in experiments are many orders of magnitude smaller than what would be needed to observe an unbinding event on the time scales accessible to molecular-dynamics simulations [4]. It is therefore worthwhile to consider simple, schematic models of bond breaking, which can be analyzed analytically and thereby help to bridge the gap between experiments and simulations.

Great effort has been put into the theoretical description of simple two-state systems with a single pathway between them [9–13], because they provide a minimal model for ligand-receptor binding kinetics and folding-unfolding transitions of single-domain proteins. Typically, the transition rates between the two states are modeled in such a way that they represent a *slip bond* [14,15], i.e., a bond that softens under external loads. However, various intermolecular bonds display, next to the expected slip events, a so-called *catch* regime [16–20], where the lifetime of the bond initially grows with the applied force up to a certain characteristic value, $F = F_{\text{char}}$ [15]. For forces beyond F_{char} , the bond eventually exhibits “normal” slip behavior. To explain this nonmonotonic force dependence, different models have been proposed [17,21,22]. One idea is that the system can follow two competing reaction pathways (a catch and a slip path, respectively) to transit between the bound and the unbound state. The two rates specifying the transition probabilities along these pathways have different force dependencies and thus dominate the reaction in different force regimes. By using phenomenological expressions [10,14] for said rates, this model has been very successful in analyzing

a broad variety of experimental data that feature anomalous force behavior [17,22]. Finally, the two-pathway model has also been generalized to include multiple bound states [17,23] to reproduce observed nonexponential reaction kinetics.

In this paper, we build upon recent advances in the mathematical description of slip bonds [13] to improve the two-pathway model and make it applicable at high and low forces and loading rates. Instead of relying on phenomenological rates, we compute the catch and slip rates microscopically. The paper is structured as follows. In Sec. II, we briefly review single- and two-pathway rate kinetics, where the former is discussed for simplicity in terms of pure slip bonds. Section III treats the cases of static and dynamic force protocols separately, giving derivations of the associated force-dependent mean lifetimes $\tau(F)$ and loading-rate dependent rupture-force distributions $p(F, \dot{F})$, which are compared to Brownian dynamics simulations. Most force transducers used in actual experiments can, to a good approximation, be represented by a relatively stiff spring attached to the bond. Nevertheless, for better clarity we have restricted our analysis in the main text to the so-called “soft-spring limit” [24], where the external forcing is solely taken into account by a linear term $-\Delta x F$ in the Hamiltonian. The extension of our results to include stiff actuators is somewhat tedious, since it requires force fluctuations to be taken into account, and it has therefore been deferred to the Appendix. We conclude in Sec. IV with a summary of our results.

II. BOND KINETICS**A. Single-pathway (slip) bonds**

In Kramers' reaction theory [9,25], the transition from a bound to an unbound state is modeled by the stochastic motion of a virtual particle, diffusing in a free-energy landscape, projected along the reaction coordinate. Bond breaking amounts to the particle overcoming a barrier that separates the states. The inclusion of an external force tilts the landscape and effectively reduces the height and width of the barrier, thus decreasing the survival probability $S(t)$ that the bond is still intact at a time t . If we neglect rebinding, as is frequently done when discussing forcible bond breaking [26], $S(t)$ is a solution to the reaction equation

$$\dot{S}(t) = -k(t, F)S(t), \quad S(0) = 1, \quad (1)$$

with the force-dependent escape rate $k(t, F)$ or $k(F)$ (for quasistatic processes). Determining $k(t, F)$ can be a

*Corresponding author: klaus.kroy@uni-leipzig.de

theoretically cumbersome task, but the fact that the spontaneous escape rate $k_0 \equiv k(F=0)$ follows Arrhenius' law [25], i.e., $k_0 \propto e^{-\beta\Delta\mathcal{E}}$ for sufficiently high barriers $\Delta\mathcal{E}$, has encouraged the use of phenomenological expressions $k(F)$, where the force dependence is solely taken into account in the dominant Arrhenius factor [3,10,14]. The Bell rate [10]

$$k_{\text{Bell}}(F) = k_0 e^{\beta\Delta x_b F}, \quad (2)$$

where Δx_b denotes the width of the undisturbed bound state, is a famous example of such simplified rate expressions. Employing the Bell rate keeps the number of fit parameters in the model to a minimum of two, namely k_0 and Δx_b , but it restricts the model to forces on the order of $(\beta\Delta x_b)^{-1}$ or less. At higher forces, the Bell rate only offers a crude approximation because it does not account for contractions of the bound state under external loads.

A more accurate rate expression can be obtained by generalizing Kramers' original work [9] to include external forces by adding a linear term $-\Delta x F(t)$ to the otherwise static bond potential $V(x)$. By restricting the shape of $V(x)$ to certain archetypal potentials, e.g., the truncated parabolic cusp potential

$$V_{\text{cusp}}(x) = \begin{cases} \Delta\mathcal{E}(\Delta x/\Delta x_b)^2, & \Delta x < \Delta x_b, \\ -\infty & \text{otherwise} \end{cases} \quad (3)$$

depicted in Fig. 1(d), the number of parameters entering this improved rate will be limited to three; next to the two parameters of the Bell rate, the barrier height $\Delta\mathcal{E}$ now enters explicitly. The microscopic rate expression

$$k_{\text{cusp}}(F) = k_0 \left[1 - \frac{\Delta x_b F}{2\Delta\mathcal{E}} \right] e^{\beta\Delta\mathcal{E}[1-(1-\Delta x_b F/2\Delta\mathcal{E})^2]}, \quad (4)$$

computed in this fashion [12], extends the theory's range of validity to intermediate forces and loading rates. However, it still fails for forces beyond the critical force $F_{\text{crit}} = 2\Delta\mathcal{E}/\Delta x_b$ that flattens out the energy barrier. Under such extreme forces, the quasistatic assumption behind Kramers' theory, which states that the thermal energy must be small in comparison to the height of the barrier, becomes invalid.

For $F > F_{\text{crit}}$, the escape process is virtually deterministic, since the particle is ballistically driven into the unbound state, and it is amenable to an analytical description, as long as one sticks with the cusp potential (3). This fact was first exploited in Ref. [11] to compute the mean rupture force for a dynamic force protocol and later in Ref. [13], where analytic approximations for the escape rate and the rupture-force distribution were derived. The theory presented in those papers becomes asymptotically exact for high forces and loading rates and reduces to the quasistatic Eq. (4) (and other results found in Ref. [12]) at low loading rates.

Notice that the rates (2) and (4) are single-pathway slip rates that increase with growing F . They can, however, be turned into catch rates by setting $\Delta x_b \rightarrow -\Delta x_b < 0$. This will also reverse the sign of the critical force. We exploit this in the following to compute microscopic expressions for the catch-slip rate of the two-pathway model.

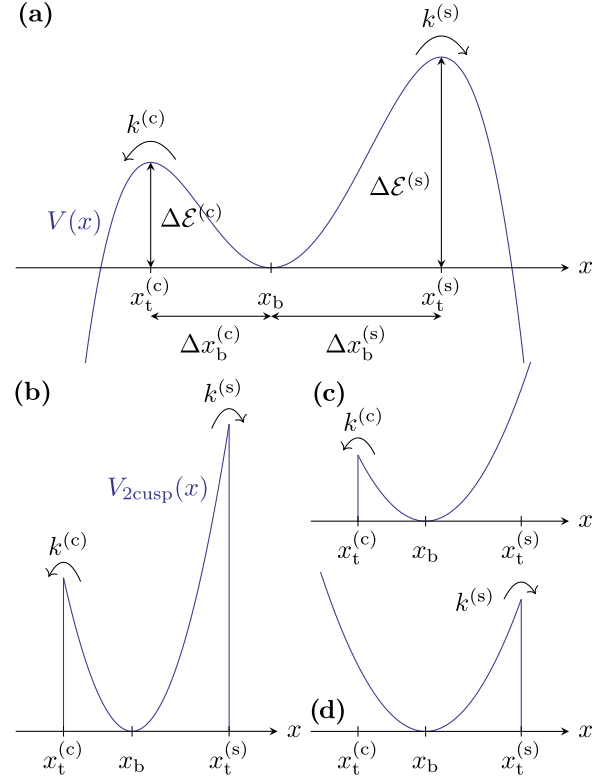


FIG. 1. A one-dimensional two-pathway free-energy landscape. (a) A virtual particle, moving in the potential $V(x)$, can either escape over the catch barrier at $x_t^{(c)}$ or over the slip barrier at $x_t^{(s)}$. The rates $k^{(c)}$ and $k^{(s)}$ depend exponentially on the barrier heights $\Delta\mathcal{E}^{(c,s)}$ and determine which pathway is more likely to be chosen. (b) The double cusp potential (9) is a schematic two-pathway landscape that does not introduce any nonlinearities into the particle's equation of motion (8). To compute the rates $k^{(c)}$ and $k^{(s)}$, the escape over each barrier is considered separately by removing one of the two absorbing boundaries, resulting in a potential with either a cusp on the left (c) or on the right (d).

B. The two-pathway model

The two-pathway model is a simple generalization of the slip bond models described above, in which the Brownian virtual particle can escape out of the potential well via two alternative pathways, as illustrated in Fig. 1(a). The survival probability still obeys Eq. (1) if $k(t, F)$ is replaced by a nonmonotonic catch-slip rate $k^{(c-s)}(t, F)$. The rate's explicit form is in general unknown, but progress can be made with the common superposition ansatz

$$k^{(c-s)}(t, F) \approx k^{(c)}(t, F) + k^{(s)}(t, F) \quad (5)$$

that approximates it by a sum of two independent single-pathway rates [22]. The formula is exact as long as at least one of the two rates is low enough to suppress events in which a virtual particle explores *both* transition states before finally escaping to the unbound state. The individual single-pathway rates in Eq. (5) can then be determined via Kramers' theory [9] [see Figs. 1(c) and 1(d)]. To allow for a nonmonotonic force dependence, such that a nontrivial solution $F_{\text{char}} > 0$ for $k^{(c)}(t, F_{\text{char}}) \equiv k^{(s)}(t, F_{\text{char}})$ exists, $k^{(c)}(t, 0)$ must be larger than

$k^{(s)}(t,0) \forall t$, which requires the catch barrier to be lower than the slip barrier [see Figs. 1(a) and 1(b)].

III. CATCH-SLIP BOND KINETICS

In single-molecule experiments, forced transitions are usually realized in two ways: either by a constant external load or by a linear force ramp. The former approach is suitable for measuring the mean lifetime $\tau(F)$ [16,18–20], which can be computed from the first-passage-time distribution $p(t, F) \equiv -\dot{S}(t)$ [27],

$$\tau(F) = \int_0^\infty dt t p(t, F) = \int_0^\infty dt S(t). \quad (6)$$

A repeated application of the linear force ramp $F(t) = \dot{F}t$, as used in Ref. [23], reveals a whole distribution of rupture forces at which the bond yields. Since the loading rate can be varied, this protocol allows us to extract even richer information about the underlying energy landscape than the static method in the form of the rupture-force distribution $p(F, \dot{F})$, which is related to the survival function $S(t)$ via [28]

$$p(F, \dot{F})dF = -\dot{S}(t)dt. \quad (7)$$

The escape rates $k^{(c,s)}(t, F) \equiv k^{(c,s)}(F(t), \dot{F})$ are now dependent on the loading rate $\dot{F} = dF/dt$, which is kept constant during each set of loading cycles. In the following, we discuss these two standard protocols separately.

A. Constant force

The virtual particle's overdamped equation of motion is

$$\frac{1}{D\beta} \dot{x}(t) = -U'(x, F) + \xi(t), \quad (8)$$

where D is the diffusion coefficient and $\xi(t)$ is Gaussian white noise with zero mean, i.e., $\langle \xi(t) \rangle = 0$ and $\langle \xi(t)\xi(t') \rangle = 2\delta(t-t')/D\beta^2$. The effective free-energy landscape $U(x, F) = V(x) - (x - x_b)F$ is composed of the bond potential $V(x)$ and the mechanical work performed by the force F . Here, we model $V(x)$ by a double-cusp potential,

$$V_{\text{cusp}}(x) = \begin{cases} \kappa_{\text{mol}}(x - x_b)^2/2, & x_t^{(c)} < x < x_t^{(s)}, \\ -\infty & \text{otherwise} \end{cases} \quad (9)$$

to facilitate the derivation of analytic expressions for common experimental observables, which are valid for arbitrary forces F and (in the case of force-ramp protocols) loading rates \dot{F} . The coordinates $x_t^{(c)}$ and $x_t^{(s)}$ stand for the transition states of the catch and slip pathway, respectively, and x_b is the location of the bound state's minimum. By design, we have $x_t^{(c)} - x_b = -\Delta x_b^{(c)} < 0$ for the catch pathway, which results in a barrier height that increases with F . Therefore, we can safely adopt the known quasistatic result (4),

$$k^{(c)}(F) = k_0^{(c)} \left[1 + \frac{F}{F_{\text{crit}}^{(c)}} \right] e^{\beta \Delta \mathcal{E}^{(c)} [1 - (1 + F/F_{\text{crit}}^{(c)})^2]}, \quad (10)$$

where $k_0^{(c)} = D\beta F_{\text{crit}}^{(c)} \sqrt{\beta \Delta \mathcal{E}^{(c)}/\pi} e^{-\beta \Delta \mathcal{E}^{(c)}/\Delta x_b^{(c)}}$ denotes the spontaneous dissociation rate, $\Delta \mathcal{E}^{(c)} = \kappa_{\text{mol}}(\Delta x_b^{(c)})^2/2$ is the initial height of the catch-pathway barrier, and $F_{\text{crit}}^{(c)} = 2\Delta \mathcal{E}^{(c)}/\Delta x_b^{(c)} \equiv \kappa_{\text{mol}}\Delta x_b^{(c)}$ gives the absolute value of the

(negatively valued) critical force that would be needed to tear it down.

The slip rate's force dependence is opposite to that of the catch rate. The corresponding barrier therefore decreases as a function of F , until the quasistatic approximation eventually breaks down. Only for small forces does the quasistatic limit hold, where the survival function is given by the expression $S(t) \sim e^{-[k^{(c)}(F) + k^{(s)}(F)]t}$ that can be used to evaluate Eq. (6),

$$\tau(F \ll F_{\text{crit}}^{(s)}) \sim \frac{1}{k^{(c)}(F) + k^{(s)}(F)}. \quad (11)$$

Here, $k^{(s)}(F)$ is the quasistatic slip escape rate,

$$k^{(s)}(F) = k_0^{(s)} \left[1 - \frac{F}{F_{\text{crit}}^{(s)}} \right] e^{\beta \Delta \mathcal{E}^{(s)} [1 - (1 - F/F_{\text{crit}}^{(s)})^2]}, \quad (12)$$

with $k_0^{(s)}$, $\Delta \mathcal{E}^{(s)}$, and $F_{\text{crit}}^{(s)}$ being defined in analogy to their catch counterparts using $\Delta x_b^{(s)} = x_t^{(s)} - x_b > 0$. At very high forces, $F \gg F_{\text{crit}}^{(s)}$, two simplifications occur. First, transitions through the slip pathway dominate the mean lifetime of the bond, which can be identified with the time it takes the particle to reach the slip transition state, i.e., $\tau(F \gg F_{\text{crit}}^{(s)})$ satisfies the relation $x(\tau) \sim x_t^{(s)}$ [11]. Secondly, the motion of the virtual particle becomes almost deterministic so that we can safely replace $x(t)$ by its mean, $\langle x(t) \rangle$. Solving the resulting equation for $\tau(F)$ leads to

$$\tau(F \gg F_{\text{crit}}^{(s)}) \sim -\frac{\Delta x_b^{(s)}}{D\beta F_{\text{crit}}^{(s)}} \ln \left(1 - \frac{F_{\text{crit}}^{(s)}}{F} \right) \\ \underset{F \rightarrow \infty}{\sim} \frac{\Delta x_b^{(s)}}{D\beta F}. \quad (13)$$

The computation of the *exact* mean lifetime of the bond, valid for all forces F , is a well-known first-passage problem and requires the solution of the differential equation

$$D e^{\beta U(x', F)} \frac{\partial}{\partial x'} e^{-\beta U(x', F)} \frac{\partial}{\partial x'} \tau(x', F) = -1, \quad (14)$$

with the initial conditions $\tau(x_t^{(c)}, F) = \tau(x_t^{(s)}, F) = 0$ [27]. Since our escape process is only one-dimensional, Eq. (14) can be solved directly by integration. Assuming that the initial position x' of the virtual particle is Boltzmann-distributed, the mean lifetime is then given by

$$\tau(F) = \frac{2}{\Delta x_b^{(s)}} \sqrt{\frac{\beta \Delta \mathcal{E}^{(s)}}{\pi}} \int_{-\Delta x_b^{(c)}}^{\Delta x_b^{(s)}} d\Delta x' \tau(x', F) \\ \times \frac{e^{-\beta \Delta \mathcal{E}^{(s)} (\Delta x'/\Delta x_b^{(s)})^2}}{\text{erf}(\sqrt{\beta \Delta \mathcal{E}^{(c)}}) + \text{erf}(\sqrt{\beta \Delta \mathcal{E}^{(s)}})}, \quad (15a)$$

where $\Delta x' = x' - x_b$. For $\beta \Delta \mathcal{E}^{(c,s)} \gg 1$, we can drop the integral over the initial condition in the above equation and just set $x' \equiv x_b$. This approximation holds for arbitrary forces, since at small forces the bond has enough time to equilibrate before it ruptures, while in the high-force limit the virtual particle is pulled deterministically out of the bound state and only its initial mean position $\langle x' \rangle = x_b$ is then of importance. We therefore get for the double-cusp potential (9) an asymptotically exact explicit expression for the mean

lifetime,

$$\begin{aligned} \tau(F) &\stackrel{\beta\Delta\mathcal{E}^{(c,s)} \gg 1}{\sim} \tau(x_b, F) \\ &= \frac{\pi (\Delta x_b^{(s)})^2}{4D\beta\Delta\mathcal{E}^{(s)}} \left(\frac{\operatorname{erfi}(A_2) - \operatorname{erfi}(A_1)}{\operatorname{erfi}(A_3) - \operatorname{erfi}(A_1)} [\psi(A_3) - \psi(A_2)] \right. \\ &\quad \left. - \frac{\operatorname{erfi}(A_3) - \operatorname{erfi}(A_2)}{\operatorname{erfi}(A_3) - \operatorname{erfi}(A_1)} [\psi(A_2) - \psi(A_1)] \right) \Big|_{x'=x_b}. \end{aligned} \quad (15b)$$

For better clarity, we have employed the following abbreviations:

$$A_1 = -\sqrt{\beta\Delta\mathcal{E}^{(c)}} \left[1 + \frac{F}{F_{\text{crit}}^{(c)}} \right], \quad (15c)$$

$$A_2 = \sqrt{\beta\Delta\mathcal{E}^{(s)}} \left[\frac{\Delta x'}{\Delta x_b^{(s)}} - \frac{F}{F_{\text{crit}}^{(s)}} \right], \quad (15d)$$

$$A_3 = \sqrt{\beta\Delta\mathcal{E}^{(s)}} \left[1 - \frac{F}{F_{\text{crit}}^{(s)}} \right], \quad (15e)$$

and, following Ref. [29],

$$\psi(z) = \underbrace{\operatorname{erf}(-A_1)}_{\beta\Delta\mathcal{E}^{(c)} \gg 1} \operatorname{erfi}(z) + \frac{2}{\sqrt{\pi}} \int_0^z dy e^{y^2} \operatorname{erf}(y), \quad (15f)$$

based on the imaginary error function $\operatorname{erfi}(z) = \operatorname{erf}(iz)/i$. Equations (15) for the mean bond lifetime under a static load F , as well as the asymptotic expressions (11) and (13), are among the main results of this paper. Similar expressions can also be obtained for harmonic force transducers, where the instrument's spring constant effectively alters the barrier heights of both pathways. We refer the interested reader to the Appendix for the results; see specifically Eqs. (A5) and (A6a).

In Fig. 2, we compare Eq. (15b) and its asymptotes to the prediction based on the phenomenological Bell rate (2),

$$\tau_{\text{Bell}}(F) = \frac{1}{k_0^{(c)} e^{-\beta\Delta x_b^{(c)} F} + k_0^{(s)} e^{\beta\Delta x_b^{(s)} F}}. \quad (16)$$

It decays exponentially, whereas our practically exact result (15b) vanishes algebraically as $F \rightarrow \infty$; see Eq. (13). The slight discrepancy between the quasistatic asymptote (11) and our exact solution (15b) at low forces is a finite-barrier-size effect, due to computing the analytic expressions (10) and (12) in the high-barrier limit. It vanishes as $\beta\Delta\mathcal{E}^{(c,s)} \rightarrow \infty$.

B. Force ramp

The equation of motion under dynamic loads has the same form as Eq. (8), with a time-dependent protocol $F(t)$ in place of the constant F , and it results in a nonstationary process $x(t)$. Specifically, we consider the force ramp $F(t) = \dot{F}t$. The quantity of interest is the rupture-force distribution [28]

$$\begin{aligned} p(F, \dot{F}) &= \frac{1}{\dot{F}} [k^{(c)}(F, \dot{F}) + k^{(s)}(F, \dot{F})] \\ &\quad \times \exp\left(-\int_0^F df \frac{k^{(c)}(f, \dot{F}) + k^{(s)}(f, \dot{F})}{\dot{F}}\right). \end{aligned} \quad (17)$$

Here, the catch rate $k^{(c)}(F, \dot{F})$ can be replaced by the quasistatic rate $k^{(c)}(F)$ for the same reasons as given in the previous

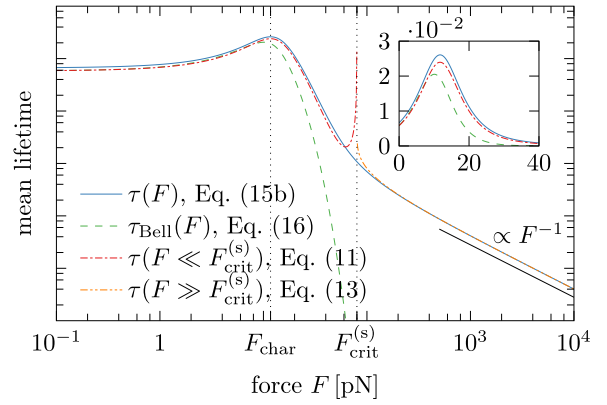


FIG. 2. The mean lifetime of a catch-slip bond under constant load using the parameters $D = 1000 \text{ nm}^2 \text{ s}^{-1}$, $\Delta x_b^{(c)} \approx 0.707 \text{ nm}$, $\Delta x_b^{(s)} = 1 \text{ nm}$, $\beta\kappa_{\text{mol}} = 20 \text{ nm}^{-2}$ (which is equivalent to setting $\beta\Delta\mathcal{E}^{(c)} = 5$ and $\beta\Delta\mathcal{E}^{(s)} = 10$), and $\beta^{-1} = 4 \text{ pN nm}$. The asymptotic expressions (red single dot-dashed line and orange double dot-dashed line) match our (virtually) exact solution $\tau(F) \sim \tau(x_b, F)$ (solid blue line) remarkably well for high and low external forces, respectively. They only deviate significantly for $F \approx F_{\text{crit}}^{(s)} = 80 \text{ pN}$. The phenomenological expression $\tau_{\text{Bell}}(F)$ (green dashed line) already breaks down around the characteristic force $F_{\text{char}} = 11.72 \text{ pN}$, and it fails at strong forces. The inset shows the maximum of the mean lifetime in a linear plot.

subsection. Since the rates for static and dynamic loading are indistinguishable in the quasistatic limit [30], we can directly employ the catch rate from Eq. (10) also for the force-ramp scenario. For the slip rate, however, a more general expression is required that accounts for the nonstationary rate-dependent character of the escape process. Following Ref. [13], we obtain

$$\begin{aligned} k^{(s)}(F, \dot{F}) &\approx k_0^{(s)} \left[1 + \frac{F}{F_{\text{crit}}^{(s)}} - \frac{2\langle\Delta x(F, \dot{F})\rangle}{\Delta x_b^{(s)}} \right] \\ &\quad \times \left[\frac{1}{2} + \frac{1}{2} \operatorname{erf}\left(\sqrt{\beta\Delta\mathcal{E}^{(s)}} \left[1 - \frac{\langle\Delta x(F, \dot{F})\rangle}{\Delta x_b^{(s)}} \right] \right) \right]^{-1} \\ &\quad \times e^{\beta\Delta\mathcal{E}^{(s)} \{1 - [1 - \langle\Delta x(F, \dot{F})\rangle/\Delta x_b^{(s)}]^2\}}, \end{aligned} \quad (18)$$

where $\langle\Delta x(F, \dot{F})\rangle = \langle x(F) \rangle - x_b$ is given by

$$\langle\Delta x(F, \dot{F})\rangle = \Delta x_b^{(s)} \left[\frac{F}{F_{\text{crit}}^{(s)}} - \frac{\Delta x_b^{(s)} \dot{F} [1 - C(F)]}{D\beta(F_{\text{crit}}^{(s)})^2} \right], \quad (19)$$

and $C(F) = e^{-D\beta F_{\text{crit}}^{(s)} F/\Delta x_b^{(s)} \dot{F}}$ is the normalized autocorrelation function of the process $x(t)$.

To improve the readability of our results, we now introduce the single-pathway rupture-force distributions $p^{(c)}(F, \dot{F}) = p(F, \dot{F})|_{k^{(s)}(F, \dot{F})=0}$ and $p^{(s)}(F, \dot{F}) = p(F, \dot{F})|_{k^{(c)}(F)=0}$ to recast Eq. (17) into the following form:

$$\begin{aligned} p(F, \dot{F}) &= \dot{F} p^{(c)}(F, \dot{F}) p^{(s)}(F, \dot{F}) \\ &\quad \times [k^{(s)}(F, \dot{F})^{-1} + k^{(c)}(F)^{-1}]. \end{aligned} \quad (20)$$

The single-pathway rupture-force distributions were originally derived in Refs. [12] and [13], but for completeness we shall

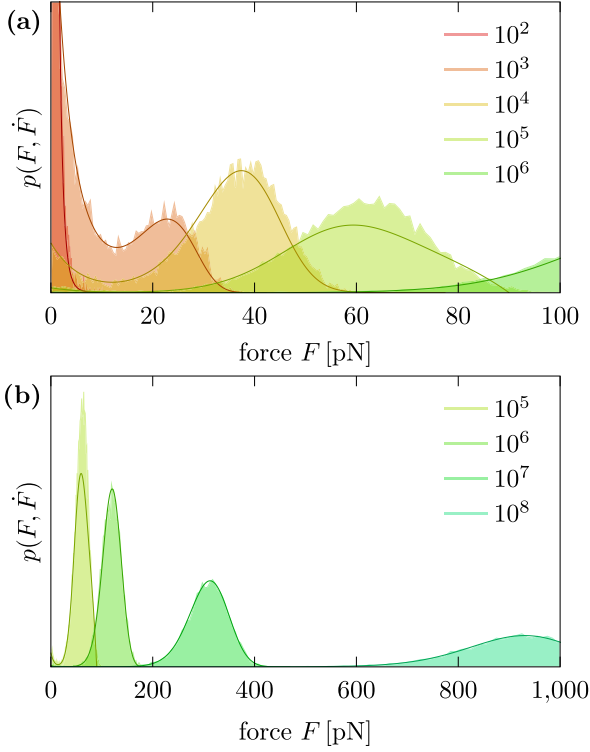


FIG. 3. The catch-slip rupture-force distribution (20) (solid lines) as a function of the loading rate (increasing from left to right), plotted on top of numerical data from Brownian dynamics simulations (shaded areas); parameters as in Fig. 2. (a) At low loading rates, the shape of the predicted distribution evolves from shoulderlike to peaked, as observed in experiments [23]. (b) For higher pulling speeds, the catch pathway becomes negligible and the rupture-force distribution becomes essentially Gaussian [7,13]. Only for loading rates in the vicinity of $\dot{F}_{\text{crit}} = 80\,000$ pN s $^{-1}$ does our approximate expression (20) exhibit sizable errors.

also present them here: the catch distribution is given by [12]

$$p^{(c)}(F, \dot{F}) = \frac{k^{(c)}(F)}{\dot{F}} e^{[k^{(c)}(F)/(1+F/F_{\text{crit}}^{(c)}) - k_0^{(c)}/\beta\Delta x_b^{(c)}] \dot{F}} \quad (21)$$

and the distribution of slip events by [13]

$$p^{(s)}(F, \dot{F}) \approx \frac{k_0^{(s)}}{\dot{F}} \left[1 + \frac{F}{F_{\text{crit}}^{(s)}} - \frac{2\langle\Delta x(F, \dot{F})\rangle}{\Delta x_b^{(s)}} \right] \times \exp\left(-\frac{k_0^{(s)}(e^{\beta\Delta\mathcal{E}^{(s)}[1-(1-F/F_{\text{crit}}^{(s)})^2]} - 1)}{\beta\Delta x_b^{(s)}\dot{F}}\right) \times e^{\beta\Delta\mathcal{E}^{(s)}\{1-[1-\langle\Delta x(F, \dot{F})\rangle/\Delta x_b^{(s)}]^2\}}. \quad (22)$$

Equations (10), (18), (21), and (22), in combination with Eq. (20), constitute the second main result of this paper. They are compared to distributions obtained from Brownian dynamics simulations in Fig. 3. Similar to our asymptotic expressions (11) and (13) for the mean lifetime, which exhibit a spurious divergence at the critical force $F_{\text{crit}}^{(s)}$, the two-pathway distribution (20) displays sizable errors near a critical loading rate, above which the catch pathway can be neglected and $p(F, \dot{F} \gg \dot{F}_{\text{crit}}) \sim p^{(s)}(F, \dot{F})$. This critical rate is the same as that found in Ref. [13], $\dot{F}_{\text{crit}} = DF_{\text{crit}}^{(s)}/(\Delta x_b^{(s)})^2$. The problems

are due to the approximations underlying Eqs. (18) and (22). Nevertheless, above and below the critical loading rate our results become asymptotically exact, in particular also in the high-loading-rate limit $\dot{F} \rightarrow \infty$ that is inaccessible to quasistatic theories. In this limit, a fourth fit parameter can be introduced to improve fits to the data, for which the underlying energy landscape deviates strongly from the cusp potential considered here, as discussed in Ref. [13]. A generalization of the above results to account for stiff actuators is given in the Appendix.

IV. CONCLUSION

In this paper, we have analyzed an analytically tractable model for catch-slip bonds, which permits arbitrarily large forces and loading rates. We represented the bond-breaking process by a one-dimensional two-pathway escape problem under external forcing using a double-cusp potential. The specific choice of the potential allowed us to compute microscopically exact escape rates, from which we then derived other experimental observables of interest. For static loads, we provided a practically exact expression for the mean lifetime that can easily be evaluated numerically [see Eq. (15b)]. Its asymptotic behavior, above and below the critical force $F_{\text{crit}}^{(s)}$, is captured by simple analytical results. For the case of a dynamic force protocol, we expressed the two-pathway rupture-force distribution $p(F, \dot{F})$ in terms of the single-pathway distributions $p^{(c)}(F, \dot{F})$ and $p^{(s)}(F, \dot{F})$, which could be adapted from the recent literature [12,13]. The resulting expression, Eq. (20), holds for both high and low loading rates. It only breaks down in a narrow region close to the critical loading rate \dot{F}_{crit} . The newly derived asymptotic results for bond breaking under high static forces or high loading rates are already (at least partially) accessible in experiments [31]. Their knowledge becomes crucial when data from molecular-dynamics simulations are compared to experimental data.

ACKNOWLEDGMENTS

We thank Sebastian Sturm for stimulating discussions and comments on the manuscript. Financial support from the European Union and the Free State of Saxony and the Leipzig School of Natural Sciences—Building with Molecules and Nano-objects (BuildMoNa) is gratefully acknowledged.

APPENDIX: SPRINGLIKE FORCE TRANSDUCERS

This appendix extends the results of the main text such that they can be directly applied to experiments and simulations that impose the external load F via intermediate force transducers of finite elasticity, e.g., AFM cantilevers, optical tweezers, or biomembranes. All these devices can accurately be modeled as harmonic springs. Sometimes, however, polymer tethers are utilized in experiments to anchor the macromolecule of interest to a substrate or to facilitate its binding to the actuator [32]. These linker molecules usually have highly nonlinear force-extension relations [30,33] that affect the effective free-energy landscape of the bond [34]. In such cases, the following results can therefore only be considered as a first approximation.

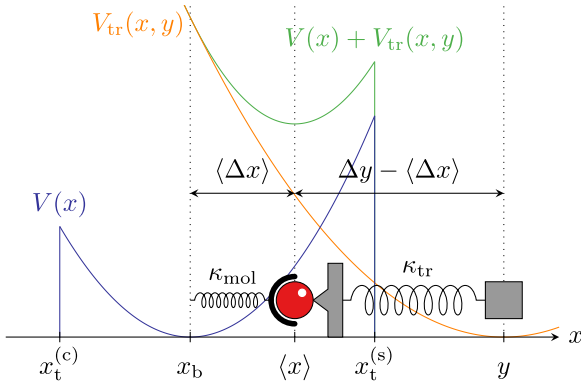


FIG. 4. Schematic figure of bond loading with a springlike force transducer. The combined system of bond (depicted as a cup and a sphere) and actuator (with a tip attached to the sphere and its base positioned at $x = y$) can be regarded as a set of harmonic springs, connected in series. For small displacements $\Delta y = y - x_b$, the reaction coordinate $x(t)$ fluctuates around the minimum of the effective potential $V(x) + V_{tr}(x, y)$ at $x = \langle x \rangle$. As $\Delta y \rightarrow \infty$, the mean bond extension $\langle \Delta x \rangle$ becomes negligible and the bond is driven deterministically toward the unbound state.

For a harmonic force transducer with an equilibrium position y that is directly imposed by external means, the mechanical work sector in the effective potential $U(x, F)$ takes the form $\kappa_{tr}[x(t) - x_b - \Delta y]^2/2$, altering the Langevin Eq. (8) for $x_t^{(c)} < x < x_t^{(s)}$ as follows:

$$\frac{1}{D\beta} \dot{x}(t) = -\chi \kappa_{mol}[x(t) - x_b] + \kappa_{tr} \Delta y + \xi(t). \quad (\text{A1})$$

Here, $\chi = 1 + \kappa_{tr}/\kappa_{mol}$, κ_{tr} is the spring constant of the transducer, and y , defined by $\Delta y = y - x_b$, is the minimum position of the transducer potential (see Fig. 4). In the case of an interposed harmonic linker with stiffness κ_{link} , κ_{tr} can be replaced by $\kappa_{eff} = (\kappa_{tr}^{-1} + \kappa_{link}^{-1})^{-1}$. A prescribed extension protocol $y = y(t)$ results in a force $F(t) = \kappa_{tr}\{\Delta y(t) - [x(t) - x_b]\}$ acting on the bond that fluctuates around the average value

$$\begin{aligned} \langle F(t) \rangle &= \kappa_{tr}[\Delta y(t) - \langle \Delta x(t, y) \rangle] \\ &= \kappa_{tr} \left[\Delta y(t) - \frac{\chi - 1}{\chi} \int_0^t d\tau \dot{C}(t - \tau) \Delta y(\tau) \right] \\ &\sim \begin{cases} \kappa_{tr} \Delta y(t), & t \ll 1/\chi D\beta \kappa_{mol}, \\ \kappa_{tr} \Delta y(t)/\chi & \text{otherwise,} \end{cases} \end{aligned} \quad (\text{A2})$$

where $\langle \Delta x(t, y) \rangle = \langle [x(t) - x_b] \rangle$ and $C(t) = e^{-\chi D\beta \kappa_{mol} t}$. In the last step, we assumed that $y(t)$ is of order $O(t)$ or less, e.g., $y = \text{const}$ or $\dot{y} = \text{const}$, which conforms to the two most common experimental scenarios, namely constant and linearly growing displacements.

It is now straightforward to generalize the central results from the main text as functions of Δy via Eq. (A1). However, in experiments and simulations, these quantities are conventionally expressed as functions of the measured force, which is in most cases equivalent to some averaged force $\langle F(t) \rangle$. The reason is that measurements “smooth out” force fluctuations, either due to a finite time resolution or by the use of low-pass filters, and therefore we shall make no distinction between

$F(t)$ and its average $\langle F(t) \rangle$ in what follows. Then we can use Eqs. (A2) to transform our results from Eqs. (6) and (7) to obtain the desired generalized expressions. Some caution must be exercised, though, because the value of the force defined in Eqs. (A2) depends on the time scale on which the bond ruptures. At lifetimes t that are much longer than the relaxation time $(\chi D\beta \kappa_{mol})^{-1}$ of the bond, the escape process is quasistatic and the system resembles two springs connected in series (hence the appearance of the effective spring constant κ_{tr}/χ) [13,24]; see Fig. 4. For increasing or more rapidly ramped-up displacements $\Delta y(t)$, the bond can at some point no longer thermalize before it fails, so that the bond’s elasticity becomes negligible relative to the viscous friction. This results in a force $F(t) \sim \kappa_{tr} \Delta y(t)$, which for stiff actuators differs significantly from the quasistatic case.

1. Constant displacement

The quasistatic approximation is applicable as long as $F \ll F_{crit}^{(s)}$. Therefore, the expressions for the asymptotic force at short and long lifetimes in Eq. (A2) translate to

$$F \sim \begin{cases} \kappa_{tr} \Delta y / \chi, & 0 \leq F \ll F_{crit}^{(s)}, \\ \kappa_{tr} \Delta y, & F \gg F_{crit}^{(s)}. \end{cases} \quad (\text{A3})$$

The quasistatic catch and slip rates then take the form [13]

$$\begin{aligned} k^{(c,s)}(F) &= \chi^{3/2} k_0^{(c,s)} \left[1 \pm \frac{F}{F_{crit}^{(c,s)}} \right] \\ &\times e^{\beta \Delta \mathcal{E}^{(c,s)} [1 - \chi (1 \pm F/F_{crit}^{(c,s)})^2]}, \end{aligned} \quad (\text{A4})$$

which we can use to evaluate Eq. (11). Using the asymptote (A3) for extreme forces, we get by solving $\langle \Delta x(t, y) \rangle = \Delta x_b^{(s)}$ the expression

$$\begin{aligned} \tau(F \gg F_{crit}^{(s)}) &\sim -\frac{\Delta x_b^{(s)}}{\chi D\beta F_{crit}^{(s)}} \ln \left(1 - \frac{\chi F_{crit}^{(s)}}{F} \right) \\ &\stackrel{F \rightarrow \infty}{\sim} \frac{\Delta x_b^{(s)}}{D\beta F}. \end{aligned} \quad (\text{A5})$$

The constant-force scenario of Sec. III can either be retrieved in the soft-spring limit, $\chi \rightarrow 1$, or by enforcing stepwise force-clamp conditions with the appropriate hardware [35]. However, such measures are only necessary in the quasistatic regime, because at sufficiently high forces the device stiffness no longer plays a role for the mean lifetime, as a comparison between Eqs. (13) and (A5) reveals.

The exact mean lifetime has the form

$$\begin{aligned} \tau(\Delta y) &= \frac{\Delta x_b^{(s)}}{2D} \sqrt{\frac{\pi}{\chi \beta \Delta \mathcal{E}^{(s)}}} \int_{-\Delta x_b^{(c)}}^{\Delta x_b^{(s)}} d\Delta x' \\ &\times \frac{e^{-\chi \beta \Delta \mathcal{E}^{(s)} (\Delta x' / \Delta x_b^{(s)})^2}}{\text{erf}(\sqrt{\chi \beta \Delta \mathcal{E}^{(c)}}) + \text{erf}(\sqrt{\chi \beta \Delta \mathcal{E}^{(s)}})} \\ &\times \left(\frac{\text{erfi}(B_2) - \text{erfi}(B_1)}{\text{erfi}(B_3) - \text{erfi}(B_1)} [\psi(B_3) - \psi(B_2)] \right. \\ &\left. - \frac{\text{erfi}(B_3) - \text{erfi}(B_2)}{\text{erfi}(B_3) - \text{erfi}(B_1)} [\psi(B_2) - \psi(B_1)] \right), \end{aligned} \quad (\text{A6a})$$

with $\psi(z)$ defined almost identically to Eq. (15f) [except for the prefactor, which reads $\text{erf}(-B_1)$] and

$$B_1 = -\sqrt{\chi\beta\Delta\mathcal{E}^{(c)}} \left[1 + \frac{\kappa_{\text{tr}}\Delta y}{\chi F_{\text{crit}}^{(c)}} \right], \quad (\text{A6b})$$

$$B_2 = \sqrt{\chi\beta\Delta\mathcal{E}^{(s)}} \left[\frac{\Delta x'}{\Delta x_b^{(s)}} - \frac{\kappa_{\text{tr}}\Delta y}{\chi F_{\text{crit}}^{(s)}} \right], \quad (\text{A6c})$$

$$B_3 = \sqrt{\chi\beta\Delta\mathcal{E}^{(s)}} \left[1 - \frac{\kappa_{\text{tr}}\Delta y}{\chi F_{\text{crit}}^{(s)}} \right]. \quad (\text{A6d})$$

The result can only be transformed into a force-dependent function in the two limits of Eq. (A3), where the force is constant and $\tau(F)$ is a solution of Eq. (14). For intermediate forces, $\tau(F)$ obeys a more complex differential equation.

2. Constant speed

We now consider a force transducer pulled with constant speed v at its end. The time-dependent extension of the effective spring, consisting of the bond and the transducer, is $\Delta y(t) = vt$. If the time resolution is high enough to determine the exact instance during which $x(t)$ crosses the transition state $x_t^{(c,s)}$ (as is in principle the case in simulations), the rupture force is defined by $F(t) = \kappa_{\text{tr}}[\Delta y(t) - \Delta x_b^{(c,s)}]$ [11,13]. However, in practice, both in experiments and simulations, the averaged force prior to yielding is recorded. We can compute it by evaluating Eq. (A2) explicitly for $\Delta y(t) = vt$,

$$\langle F(t) \rangle \equiv \kappa_{\text{tr}}v \left[t - \frac{\chi - 1}{\chi} \left(t - \frac{[1 - C(t)]}{\chi D\beta\kappa_{\text{mol}}} \right) \right]. \quad (\text{A7})$$

Here, the autocorrelation function $C(t)$ is the same as that for constant displacements.

Equation (A7) can be inverted analytically to obtain a function $t(F)$, which is then used to compute the catch and slip rupture-force distributions $p^{(c,s)}(F, v)$ from the associated first-passage-time distributions $p^{(c,s)}(t, v) \equiv -\dot{S}(t)$. In the limits $\kappa_{\text{tr}}v \gg \chi\dot{F}_{\text{crit}}$ and $\kappa_{\text{tr}}v \ll \chi\dot{F}_{\text{crit}}$, the force is simply a linear function of t [13] making the inversion $t(F) \propto F$ trivial, whereas for intermediate times (and speeds) the full inverse function

$$t(F) = \frac{W[(\chi - 1)e^{\chi^{-1}C(\chi F/\kappa_{\text{tr}}v)]}{\chi D\beta\kappa_{\text{mol}}} + \frac{\chi F}{\kappa_{\text{tr}}v} - (\chi - 1)(\chi D\beta\kappa_{\text{mol}})^{-1} \quad (\text{A8})$$

must be taken into consideration. The Lambert W function $W(z)$ can be approximated by [36]

$$W(z) \approx \ln(1+z) \left[1 - \frac{\ln[1 + \ln(1+z)]}{2 + \ln(1+z)} \right] \quad (\text{A9})$$

to speed up the numerics, if necessary.

Following the arguments given above, the time-dependent catch rate can be read off Eqs. (A3) and (A4) with the

substitution $\Delta y \rightarrow \Delta y(t) = vt$,

$$k^{(c)}(t, v) = \chi^{3/2}k_0^{(c)} \left[1 + \frac{\kappa_{\text{tr}}vt}{\chi F_{\text{crit}}^{(c)}} \right] \times e^{\beta\Delta\mathcal{E}^{(c)}[1 - \chi(1 + \kappa_{\text{tr}}vt/\chi F_{\text{crit}}^{(c)})^2]}. \quad (\text{A10})$$

The slip rate is approximately given by [13]

$$k^{(s)}(t, v) \approx \chi^{3/2}k_0^{(s)} \left[1 + \frac{\kappa_{\text{tr}}vt}{\chi F_{\text{crit}}^{(s)}} - \frac{2\langle\Delta x(t, v)\rangle}{\Delta x_b^{(s)}} \right] \times \left[\frac{1}{2} + \frac{1}{2} \text{erf} \left(\sqrt{\chi\beta\Delta\mathcal{E}^{(s)}} \left[1 - \frac{\langle\Delta x(t, v)\rangle}{\Delta x_b^{(s)}} \right] \right) \right]^{-1} \times e^{\beta\Delta\mathcal{E}^{(s)}[1 - \chi(1 - \langle\Delta x(t, v)\rangle/\Delta x_b^{(s)})^2]}, \quad (\text{A11})$$

where $\langle\Delta x(t, v)\rangle$ is the same as in Eq. (A7),

$$\langle\Delta x(t, v)\rangle = \Delta x_b^{(s)} \left[\frac{\kappa_{\text{tr}}vt}{\chi F_{\text{crit}}^{(s)}} - \frac{\kappa_{\text{tr}}v\Delta x_b^{(s)}[1 - C(t)]}{\chi^2 D\beta(F_{\text{crit}}^{(s)})^2} \right]. \quad (\text{A12})$$

These expressions can be used to determine the corresponding single-pathway first-passage-time distributions with the formalism presented in Ref. [13]. For a pure catch escape, we get the distribution

$$p^{(c)}(t, v) = k^{(c)}(t, v) e^{k^{(c)}(t, v)/\beta\Delta x_b^{(c)}\kappa_{\text{tr}}v(1 + \kappa_{\text{tr}}vt/\chi F_{\text{crit}}^{(c)})} \times e^{-k^{(c)}(0, v)/\beta\Delta x_b^{(c)}\kappa_{\text{tr}}v} \quad (\text{A13})$$

and, along the slip pathway,

$$p^{(s)}(t, v) \approx \chi^{3/2}k_0^{(s)} \left[1 + \frac{\kappa_{\text{tr}}vt}{\chi F_{\text{crit}}^{(s)}} - \frac{2\langle\Delta x(t, v)\rangle}{\Delta x_b^{(s)}} \right] \times \exp \left(- \frac{\chi^{3/2}k_0^{(s)} e^{\beta\Delta\mathcal{E}^{(s)}[1 - \chi(1 - \kappa_{\text{tr}}vt/\chi F_{\text{crit}}^{(s)})^2]}}{\beta\Delta x_b^{(s)}\kappa_{\text{tr}}v} \right) \times \exp \left(\frac{\chi^{3/2}k_0^{(s)} e^{\beta\Delta\mathcal{E}^{(s)}(1 - \chi)}}{\beta\Delta x_b^{(s)}\kappa_{\text{tr}}v} \right) \times e^{\beta\Delta\mathcal{E}^{(s)}[1 - \chi(1 - \langle\Delta x(t, v)\rangle/\Delta x_b^{(s)})^2]}. \quad (\text{A14})$$

Finally, in analogy with Eq. (20), we arrive at the two-pathway rupture-force distribution $p(F, v)$ in terms of the single-pathway distributions,

$$p(F, v) = \left[\frac{d}{dt} F(t) \right]^{-1} p(t(F), v) = \frac{\chi}{\kappa_{\text{tr}}v} \frac{p^{(c)}(t(F), v)p^{(s)}(t(F), v)}{1 + (\chi - 1)C(t(F))} \times [k^{(s)}(t(F), v)^{-1} + k^{(c)}(t(F), v)^{-1}], \quad (\text{A15})$$

where $t(F)$ is given by Eq. (A8). Notice that $p(F, v)$ depends on v only via the nominal loading rate $\kappa_{\text{tr}}v$ of the force transducer, which replaces the loading rate \dot{F} as an external control parameter.

[1] J. N. Onuchic and P. G. Wolynes, *Curr. Opin. Struct. Biol.* **14**, 70 (2004).

[2] M. Gralka and K. Kroy, *Biochim. Biophys. Acta* **1853**, 3025 (2015).

- [3] C. Zhu, G. Bao, and N. Wang, *Annu. Rev. Biomed. Eng.* **2**, 189 (2000).
- [4] M. Rief and H. Grubmüller, *ChemPhysChem* **3**, 255 (2002).
- [5] W. J. Greenleaf, M. T. Woodside, E. A. Abbondanzieri, and S. M. Block, *Phys. Rev. Lett.* **95**, 208102 (2005).
- [6] A. Borgia, P. M. Williams, and J. Clarke, *Annu. Rev. Biochem.* **77**, 101 (2008).
- [7] R. Merkel, P. Nassoy, A. Leung, K. Ritchie, and E. Evans, *Nature (London)* **397**, 50 (1999).
- [8] E. Evans, *Annu. Rev. Biophys. Biomol. Struct.* **30**, 105 (2001).
- [9] H. A. Kramers, *Physica* **7**, 284 (1940).
- [10] G. I. Bell, *Science* **200**, 618 (1978).
- [11] G. Hummer and A. Szabo, *Biophys. J.* **85**, 5 (2003).
- [12] O. K. Dudko, G. Hummer, and A. Szabo, *Phys. Rev. Lett.* **96**, 108101 (2006).
- [13] J. T. Bullerjahn, S. Sturm, and K. Kroy, *Nat. Commun.* **5**, 4463 (2014).
- [14] M. Dembo, D. C. Torney, K. Saxman, and D. Hammer, *Proc. R. Soc. London, Ser. B* **234**, 55 (1988).
- [15] W. E. Thomas, V. Vogel, and E. V. Sokurenko, *Annu. Rev. Biophys.* **37**, 399 (2008).
- [16] B. T. Marshall, M. Long, J. W. Piper, T. Yago, R. P. McEver, and C. Zhu, *Nature (London)* **423**, 190 (2003).
- [17] W. E. Thomas, M. Forero, O. Yakovenko, L. Nilsson, P. Vicini, E. V. Sokurenko, and V. Vogel, *Biophys. J.* **90**, 753 (2006).
- [18] B. Guo and W. H. Guilford, *Proc. Natl. Acad. Sci. USA* **103**, 9844 (2006).
- [19] S. Rakshit, Y. Zhang, K. Manibog, O. Shafraz, and S. Sivasankar, *Proc. Natl. Acad. Sci. USA* **109**, 18815 (2012).
- [20] C. Lee, J. Lou, K. Wen, M. McKane, S. G. Eskin, S. Ono, S. Chien, P. A. Rubenstein, C. Zhu, and L. V. McIntire, *Proc. Natl. Acad. Sci. USA* **110**, 5022 (2013).
- [21] D. Bartolo, I. Derényi, and A. Ajdari, *Phys. Rev. E* **65**, 051910 (2002).
- [22] Y. V. Pereverzev, O. V. Prezhdo, M. Forero, E. V. Sokurenko, and W. E. Thomas, *Biophys. J.* **89**, 1446 (2005).
- [23] E. Evans, A. Leung, V. Heinrich, and C. Zhu, *Proc. Natl. Acad. Sci. USA* **101**, 11281 (2004).
- [24] A. Maitra and G. Arya, *Phys. Rev. Lett.* **104**, 108301 (2010).
- [25] P. Hänggi, P. Talkner, and M. Borkovec, *Rev. Mod. Phys.* **62**, 251 (1990).
- [26] R. Merkel, *Phys. Rep.* **346**, 343 (2001).
- [27] C. W. Gardiner, *Handbook of Stochastic Methods for Physics, Chemistry and the Natural Sciences* (Springer-Verlag, Berlin, 1985).
- [28] C. Friedsam, A. K. Wehle, F. Kühner, and H. E. Gaub, *J. Phys. Condens. Matter* **15**, S1709 (2003).
- [29] B. U. Felderhof, *Physica A* **387**, 1767 (2008).
- [30] O. K. Dudko, G. Hummer, and A. Szabo, *Proc. Natl. Acad. Sci. USA* **105**, 15755 (2008).
- [31] F. Rico, L. Gonzalez, I. Casuso, M. Puig-Vidal, and S. Scheuring, *Science* **342**, 741 (2013).
- [32] W. J. Greenleaf, M. T. Woodside, and S. M. Block, *Annu. Rev. Biophys. Biomol. Struct.* **36**, 171 (2007).
- [33] C. Ray, J. R. Brown, and B. B. Akhremitchev, *J. Phys. Chem. B* **111**, 1963 (2007).
- [34] A. Maitra and G. Arya, *Phys. Chem. Chem. Phys.* **13**, 1836 (2011).
- [35] M. Schlierf, H. Li, and J. M. Fernández, *Proc. Natl. Acad. Sci. USA* **101**, 7299 (2004).
- [36] S. Winitzki, in *Computational Science and Its Applications—ICCSA 2003*, Lecture Notes in Computer Science Vol. 2667 (Springer-Verlag, Berlin, 2003), pp. 780–789.